*Int. J. Heat Mass Transfer.* Vol. 32, No. 11, pp. 2027–2036, 1989
Printed in Great Britain

0017–9310/89 $3.00 + 0.00


# A numerical study of heat and momentum transfer for flexible tube bundles in cross flow

YEON CHANG,† ANTHONY N. BERIS‡ and EFSTATHIOS E. MICHAELIDES†§

†Department of Mechanical Engineering, University of Delaware, Newark, DE 19716, U.S.A.
‡Department of Chemical Engineering, University of Delaware, Newark, DE 19716, U.S.A.

(*Received* 2 *November* 1988 *and in final form* 27 *January* 1989)

**Abstract**—A numerical scheme is developed in order to calculate the heat transfer and pressure drop coefficients in heat exchangers made of flexible tubes. The vibrating tubes are modeled in a quasistatic way by taking the first tube of the row to be in 15 asymmetric (with finite eccentricity) positions with respect to the rest of the tubes and averaging in time the steady-state solutions corresponding to each one of these geometries. The results show that the eccentricity of the first tube affects the velocity and temperature profiles significantly. The time-averaged heat transfer and pressure drop coefficients are higher than those for the case of rigid, symmetrically placed, tube bundles. Comparison of the present results shows very good agreement with experimental data from flexible tube heat exchangers.

## 1. INTRODUCTION

IN GENERAL heat exchanger tube bundles are made of high stiffness materials. Vibrations have been found to induce tube wear and failure in metal tubes. Because of this, vibrations in tube bundles are minimized in well-designed heat exchangers. However, another consequence of tube vibrations is higher heat transfer caused by increased fluid mixing. Recently tube bundles made of Teflon material have been used in heat exchangers operating in corrosive environments. Teflon tubes are ideal for use in such environments because Teflon is not attacked by most corrosive fluids including strong acids, is strong enough to withstand moderately high temperatures and pressures and resists scaling. Thus, the use of heat exchangers made of Teflon and other plastics is becoming common practice for many industrial processes such as economizing heat in fossil fuel power plants with high sulfur content, heat extraction from chemical processes involving strong acids or bases and cooling hot gaseous streams carrying condensible corrosive substances.

Teflon is a flexible material and tubes made of this substance vibrate freely when they are in cross flow. Experimental studies [1, 2] with Teflon heat exchangers showed that the amplitude of vibrations is of the same order of magnitude as the diameter of the tubes. It was also found that there is a considerable increase in the average outside heat transfer coefficient and in the pressure drop of the tube bundle because of the fluid mixing that is caused by the vibrations.

Although there are several analytical and numerical studies on rigid (metal) tube heat exchangers [3–6] there is no such study on tube bundles made of flexible and freely vibrating tubes. Studies of peripheral interest are those by Telionis and Romaniuk [7] who examined numerically flows with oscillating boundary layers and by Greiner *et al.* [8] who studied the heat transfer in a resonating cavity.

A numerical or analytical study of tube bundles with high amplitude of vibrations has not yet been reported, perhaps because of the complexity and unfamiliarity of the subject. A complete study of the phenomenon involves the solution of the time-dependent Navier–Stokes equations with fluid–tube interactions which represents a very difficult task. This cannot be accomplished at the present state of computational resources even if only one tube existed. A less ambitious approach was followed in this project by adopting a quasi-steady technique. The time-averaged solution to the time-dependent flow problem is approximated by taking the first tube of the row to be in 15 positions with finite eccentricity with respect to the rest of the tubes and by averaging in time the steady-state solutions corresponding to each one of these geometries. The steady-state solutions to the particular problems arising from the various locations of the first tube were obtained by utilizing a numerical procedure.

The key idea behind this approach is to allow the use of a two-dimensional steady-state finite-element program in the numerical solution of the momentum and heat transfer of a flexible tube bundle in cross flow. The numerical technique for the solution of each of the so-generated steady-state problems is the Galerkin weighted residuals method with bilinear basis functions and streamline/vorticity formulation. This technique was also successfully used for the prediction of the heat transfer and pressure drop in rigid tubes [6]. The numerical solution is obtained for a group of five tubes in a row and can be generalized to bundles of more than five tubes in a square or triangular arrangement.

§Author to whom correspondence should be addressed.

## NOMENCLATURE

| | |
|---|---|
| $f'$ | pressure drop coefficient |
| $G$ | mass flux |
| $j$ | modified Colburn $j$-factor |
| $N$ | number of tubes in column |
| $Nu$ | Nusselt number |
| $P$ | dimensionless pressure |
| $Pr$ | Prandtl number |
| $Re$ | Reynolds number |
| $T$ | temperature |
| $u$ | longitudinal velocity [dimensionless] |
| $\Delta u_i$ | incremental value of the dependent variables |
| $U$ | inlet velocity |
| $v$ | radial velocity [dimensionless] |
| $x$ | longitudinal distance |
| $y$ | normal to the boundary coordinate. |

Greek symbols

| | |
|---|---|
| $\varepsilon$ | convergence criterion |
| $\theta$ | dimensionless temperature |
| $\rho$ | density |
| $\phi_i$ | finite element basis function |
| $\psi$ | stream function [dimensionless] |
| $\omega$ | vorticity [dimensionless] |
| $\Omega_h^e$ | computational domain |
| $\partial\Omega_h^e$ | boundary of the computational domain. |

Subscript

| | |
|---|---|
| h | finite element approximation. |

## 2. PROBLEM FORMULATION

Mach numbers in heat exchanger applications are low enough for the fluid to be considered incompressible. Typical heat exchanger tubes have also very high length to diameter ratios ($l/d > 40$) so the outside flow can be considered two-dimensional. Previous studies have also shown [5, 6, 10] that the steady-state solution yields reliable results for the pressure drop and the heat transfer in rigid tube bundles up to Reynolds numbers of 1000 despite the presence of downstream vortices.

In the case of flexible tube heat exchangers made of Teflon it was observed experimentally [2, 11] that the Strouhal numbers of the flows examined were in the range 0.002–0.008. This signifies that the tube vibrating velocity is well below the free stream velocity. Therefore, the flow can be considered quasi-steady. Furthermore, it was observed that it was the first row of the tubes that vibrated most visibly and with much higher amplitude than the other rows. For this reason, in the present study of flow through five rows of flexible tubes, it is assumed that only the first row tubes vibrate, while the others remain still.

A physical picture of the flow domain is shown in Fig. 1. Due to the symmetry of the flow, the solution is calculated for the region shown within the dotted lines. The mode of vibration of the first row of cylinders considered is such that the symmetry assumed in the computational domain is preserved. It must be emphasized here that the present study makes use of the above simplifying assumptions in order to obtain approximations to the time-averaged results of engineering interest. The solution to the full three-dimensional time-dependent problem is still beyond the capabilities of state of the art computers.

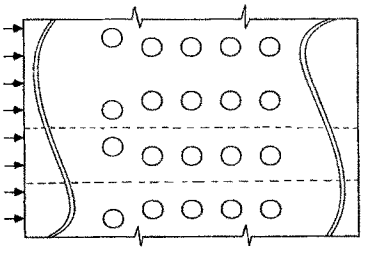

FIG. 1. A five row model for a tube bank with leading cylinder vibrating.

The conservation equations for the flow under the previously stated assumptions are given in their dimensionless form, in a Cartesian frame of reference $x$, $y$ as follows.

Continuity

$$\frac{\partial u}{\partial x}+\frac{\partial v}{\partial y}=0. \tag{1}$$

Momentum

$$u\frac{\partial u}{\partial x}+v\frac{\partial u}{\partial y}=-\frac{\partial P}{\partial x}+\frac{1}{Re}\left(\frac{\partial^2 u}{\partial x^2}+\frac{\partial^2 u}{\partial y^2}\right) \tag{2}$$

$$u\frac{\partial v}{\partial x}+v\frac{\partial v}{\partial y}=-\frac{\partial P}{\partial y}+\frac{1}{Re}\left(\frac{\partial^2 v}{\partial x^2}+\frac{\partial^2 v}{\partial y^2}\right). \tag{3}$$

Energy

$$u\frac{\partial \theta}{\partial x}+v\frac{\partial \theta}{\partial y}=\frac{1}{Re\,Pr}\left(\frac{\partial^2 \theta}{\partial x^2}+\frac{\partial^2 \theta}{\partial y^2}\right). \tag{4}$$

In the above equations the velocities are made dimensionless by dividing by the upstream velocity $U$ and the coordinates d$y$ dividing by the tube diameter $d$. The dimensionlesss parameter $\theta$ and $P$ are defined as

$$\theta=\frac{T-T_{in}}{T_w-T_{in}} \tag{5a}$$

$$P = \frac{2P^*}{\rho U^2} \tag{5b}$$

and the Reynolds number is defined with respect to $U$ and $d$.

The pressure gradient term in the momentum equations is eliminated by cross-differentiation and subtraction. The resulting equation is then given in terms of the dimensionless vorticity as follows:

$$u\frac{\partial\omega}{\partial x} + v\frac{\partial\omega}{\partial y} = \frac{1}{Re}\left(\frac{\partial^2\omega}{\partial x^2} + \frac{\partial^2\omega}{\partial y^2}\right). \tag{6}$$

The continuity equation is automatically satisfied by the stream function $\psi$. Following standard methods the stream function equation is recast in terms of the vorticity as an elliptic equation of the Poisson type

$$\frac{\partial^2\psi}{\partial x^2} + \frac{\partial^2\psi}{\partial y^2} = -\omega. \tag{7}$$

Auxiliary equations are used to obtain the velocities $u$ and $v$ for the flow field and the pressure field. The two velocities may be obtained from the vorticity function by solving the following two Poisson equations:

$$\frac{\partial^2 u}{\partial x^2} + \frac{\partial^2 u}{\partial y^2} = -\frac{\partial\omega}{\partial y} \tag{8a}$$

and

$$\frac{\partial^2 v}{\partial x^2} + \frac{\partial^2 v}{\partial y^2} = \frac{\partial\omega}{\partial x}. \tag{8b}$$

For the pressure one may also obtain a Poisson equation by cross-differentiating and adding the two momentum equations. The resulting expression is

$$\frac{\partial^2 P}{\partial x^2} + \frac{\partial^2 P}{\partial y^2} = 2\left[\frac{\partial u}{\partial x}\frac{\partial v}{\partial y} - \frac{\partial v}{\partial x}\frac{\partial u}{\partial y}\right]. \tag{9}$$

The computational domain of the flow is depicted in Fig. 2. The boundary conditions for the variables are defined in the following paragraphs. It must be noted that the non-trivial boundary conditions for the vorticity, are specified in detail in Section 3.

At the inlet ($x = 0$) a free stream flow is assumed

$$\psi = y; \quad \omega = f_1(\psi,\omega); \quad \theta = v = 0;$$
$$u = 1; \quad \partial P/\partial x = -Re^{-1}\,\partial\omega/\partial y. \tag{10a}$$

At the upper boundary ($y = 2$) the symmetry conditions are the boundary conditions

$$\psi = 1; \quad \omega = \partial\theta/\partial y = \partial u/\partial y = v = \partial P/\partial y = 0. \tag{10b}$$

At the outlet ($x = L$) fully developed flow and temperature profiles are assumed

$$\partial\psi/\partial x = \partial\omega/\partial x = \partial\theta/\partial x = \partial u/\partial x = \partial v/\partial x = 0;$$
$$\partial P/\partial x = \omega v - Re^{-1}\,\partial\omega/\partial y. \tag{10c}$$

On the lower symmetry line ($y = 0$) the following symmetry conditions are applicable:

$$\psi = -1, \quad \omega = \partial\theta/\partial y = \partial u/\partial y = v = \partial P/\partial y = 0. \tag{10d}$$

Finally, at the surface of the tubes ($r = 0.5$), the nonslip conditions are used

$$\omega = f_2(\psi,\omega); \quad \theta = 1; \quad u = v = 0;$$
$$\partial P/\partial r = -\,Re^{-1}\,r^{-1}\partial\omega/\partial\phi \tag{10e}$$

where $r, \phi$ refer to the local for each tube cylindrical coordinate system with its center at the center of the tube.

The case of the vibrating tubes differs from the case of the rigid tubes in the stream function boundary condition at the surface of the tubes. In the case of rigid tubes [9, 10] one knows the value of the stream function on the tube boundaries (usually set to zero) because the problem has an additional symmetry condition. However, in the case of vibrating cylinders the values of the stream function on the solid tubes are unknown. Therefore, the stream function boundary values have to be calculated simultaneously with the values in the flow domain by using an additional constraint equation. The last equation is derived from the pressure values along the solid body boundary as will be shown in Section 3.

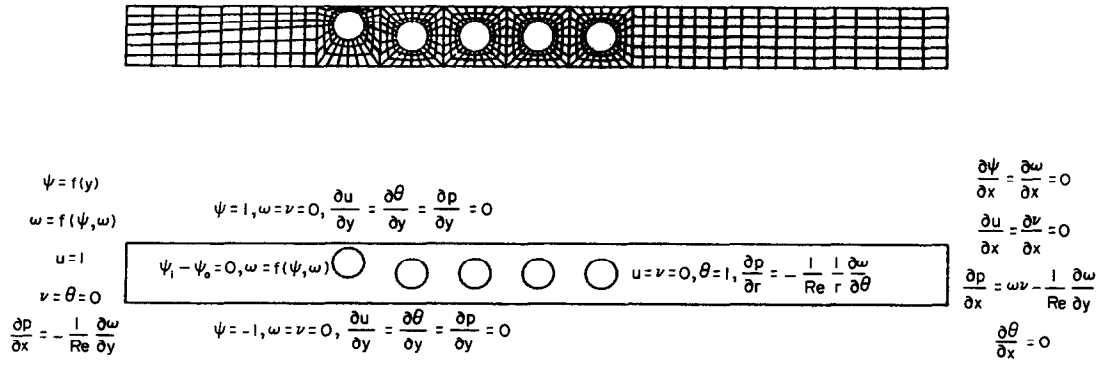


FIG. 2. Computational domain with boundary conditions.

Starting from the conservation equations the Galerkin weighted residuals are formed according to standard procedure [12]. The same bilinear basis functions, $\phi_i$, have been used for the finite-element approximations and also as the weighing functions in all equations. The normal derivative (Von Neumann) boundary conditions have been used to eliminate the surface integrals at the inlet, outlet and symmetry lines and to bring the resulting discrete equations to their final form. Following this procedure the final form of the vorticity and stream function equations are

$$\int_{\Omega_h^e}\left\{\left[\frac{\partial\psi_h}{\partial y}\frac{\partial\omega_h}{\partial x}-\frac{\partial\psi_h}{\partial x}\frac{\partial\omega_h}{\partial y}\right]\phi_i - \frac{1}{Re}\nabla\omega_h\cdot\nabla\phi_i\right\}dx = 0 \quad (11)$$

$$\int_{\Omega_h^e}\{\nabla\psi_h\cdot\nabla\phi_i-\omega_h\phi_i\}\,dx = 0 \quad (12)$$

where $\phi_i$ is the finite-element weighing function and subscript h denotes the finite-element approximation to the corresponding variable. Similarly the final form of the energy equation is

$$\int_{\Omega_h^e}\left\{\left[u_h\frac{\partial\theta_h}{\partial x}+v_h\frac{\partial\theta_h}{\partial y}\right]\phi_i + \frac{1}{Re\,Pr}\left[\frac{\partial\theta_h}{\partial x}\frac{\partial\phi_i}{\partial x}+\frac{\partial\theta_h}{\partial y}\frac{\partial\phi_i}{\partial y}\right]\right\}dx = 0. \quad (13)$$

Finally, the three auxiliary equations for the two velocities $u$ and $v$ and the pressure $P$ are as follows:

$$\int_{\Omega_h^e}\left\{\nabla u_h\cdot\nabla\phi_i-\frac{\partial\omega_h}{\partial y}\phi_i\right\}dx = 0 \quad (14a)$$

$$\int_{\Omega_h^e}\left\{\nabla v_h\cdot\nabla\phi_i+\frac{\partial\omega_h}{\partial x}\phi_i\right\}dx = 0 \quad (14b)$$

$$\int_{\Omega_h^e}\left\{2\left[\frac{\partial v_h}{\partial y}\frac{\partial u_h}{\partial x}-\frac{\partial v_h}{\partial x}\frac{\partial u_h}{\partial y}\right]\phi_i + \nabla P_h\cdot\nabla\phi_i\right\}dx - \int_{\partial\Omega_h^e}\frac{\partial P_h}{\partial n}\phi_i\,ds = 0. \quad (14c)$$

It must be pointed out that the surface integral in the last equation does not vanish and has to be evaluated using the non-homogeneous boundary conditions for the normal derivative of the pressure indicated in equation (10)—the boundary conditions for the pressure are of the Von Neumann type at all the surfaces. The surface integrals do not contribute in the rest of the equations, because the boundary conditions for the rest of the variables, depending on the boundary, are either of the essential (Dirichlet) type, or of the Von Neumann type corresponding to zero normal derivatives (natural boundary conditions). More details about the derivation of the equations and their discretization may be found in ref. [10].

## 3. NUMERICAL IMPLEMENTATION

One of the major difficulties for the implementation of the vorticity/stream function formulation of the conservation equations is that at the inlet and solid walls the boundary conditions of the vorticity function—the functions $f_1$ and $f_2$—are unknown [11]. In the present work the essential boundary conditions for the vorticity are expressed in terms of a relationship between the stream function and vorticity values at the boundary and the values next to the boundary nodal points. This relationship, developed in parallel to the finite difference applications [9, 13], (function $f_2$) becomes

$$\omega_w = -\frac{1}{2}\omega_{w+1}+3\frac{\psi_{w+1}-\psi_w}{h^2} \equiv f_2(\psi,\omega). \quad (15)$$

Similarly, the vorticity function at the inlet (function $f_1$) is obtained as follows:

$$\omega_i = -\frac{1}{2}\omega_{i+1}+3\frac{\psi_{i+1}-\psi_i}{h^2} \equiv f_1(\psi,\omega). \quad (16)$$

Another unknown boundary condition is the condition at the surfaces of the cylinders, as was pointed out in the previous section. On this surface the radial and azimuthal fluid velocities are zero and, therefore, equation (3) yields the following expression for the pressure gradient:

$$\frac{1}{r}\frac{\partial P}{\partial\theta} = \frac{1}{Re}\left[\frac{\partial}{\partial r}\left\{\frac{1}{r}\frac{\partial}{\partial r}(rv_\theta)\right\}\right] \quad (17)$$

where $r,\theta$ are the cylindrical coordinates and $v_\theta$ the azimuthal velocity in a local coordinate system centered at the corresponding tube center. After substituting for the vorticity equation in cylindrical coordinates in equation (17) and using again the zero velocity values on the tube surfaces one obtains

$$\frac{1}{r}\frac{\partial P}{\partial\theta} = \frac{1}{Re}\left[\frac{\partial\omega}{\partial r}+\frac{1}{r}\frac{\partial}{\partial\theta}\left(\frac{\partial v_r}{\partial r}\right)\right] \quad (18)$$

where $v_r$ is the radial velocity in cylindrical coordinates for the same tube-centered coordinate system. According to the continuity equation the second term in square brackets vanishes at the surface of the tube. When the remaining terms of equation (18) are integrated with respect to $\theta$ over a circle, the following expression is derived:

$$0 = \Delta P = \int_0^{2\pi}\left\{\frac{\partial\omega}{\partial r}r\right\}d\theta. \quad (19)$$

The last equation is used, in addition to the stream function boundary condition at the tube walls, in order to solve for the unknown value of the stream function there. The fact that the stream function does not appear explicitly in equation (19) does not matter since in the Newton–Raphson method employed here, the two variables—$\psi$ and $\omega$—coupled through equations (6) and (7), are solved for simultaneously. The

final result is that the number of unknowns is the same as the number of equations and, hence, the problem has a unique solution.

The equations resulting from the application of the Galerkin finite element method are nonlinear and need to be solved by iteration. In this study the Newton–Raphson method is used to solve simultaneously for the two primary variables, stream function and vorticity. When these two variables are determined the two velocity components are calculated by direct solution of the linear equations obtained from the Poisson equations (equations (14a) and (14b)). The energy equation is solved separately, since it is not coupled directly to the momentum equation. The calculated velocity values are used with equation (13) to obtain the dimensionless temperature $\theta$.

The pressure field is obtained by a similar method. However, because the pressure boundary conditions are of the Von Neumann type it is necessary to include the line integral terms in the finite element formulation of the pressure equation (14c). In this case the boundary conditions are expressed in terms of the velocities and their derivatives.

In order to take into account the tube vibrations a quasistatic approach is adopted. Calculations are performed with the first tube at positions ranging from 0.35 to $-0.35$ diameters off-center with steps of 0.05 diameters. These extreme values are deduced from the experiments performed with the Teflon tubes as being representative of the displacement of tubes during vibration. Thus, the time-average quantities of interest are calculated as the average of the 15 positions of the first tube.

More details about the mathematical calculations, the numerical implementation of the problem and the procedures adopted for the solution may be found in ref. [10].

## 4. RESULTS AND OBSERVATIONS

### 4.1. *Validation of the method*

The numerical scheme outlined above was first tested with the known analytical solution of Poiseuille flow between two infinite parallel plates and for a given pressure drop. One of the two symmetrical parts of the flow was calculated. To test the multiple connected domain formulation of the numerical method the flow rate at the entrance was specified within a constant, which is the value of the stream function on the solid boundary. For the exit boundary condition, a natural boundary condition in the weak formulation of the Galerkin method was used. For the final constraint on the stream function, equation (19) was used (with the integration limits modified to be from 0 to $L$). The convergence criterion for the numerical scheme was taken as

$$\max |\Delta u_i| < \varepsilon \qquad (20)$$

where $\Delta u_i$ is the incremental value of the dependent variables at the $i$th nodal point. In the calculations, $\varepsilon$ was taken to be $10^{-5}$.

The results from the numerical method were compared with those obtained analytically. In general, the solutions converged after three iterations for a mesh with 528 elements and 648 nodal points. The observed differences in the velocities, for several Reynolds numbers, were after the sixth decimal point. Even when a coarser mesh was used, the comparison between the numerical and analytical results was very good.

A mesh sensitivity analysis was performed for the solution of the rigid cylinders case where essentially the same technique was used as for the Poiseuille flow in a channel. The results from this analysis are depicted in Fig. 3. It may be seen that in the rigid tube case, a grid of 324 nodes and 240 elements was adequate for the calculation of the global quantities of interest.

### 4.2. *Results*

For the quasistatic calculations 15 positions of the first cylinder have been considered. Given that the results of seven positions can be anticipated from the symmetry of the physical domain, calculations were only made for the remaining eight positions. For each one of the eight positions computations were made for twelve Reynolds numbers between 64 and 1495.

In the symmetric configuration the exact value of the stream function at the wall is zero. The results for the vibrating cylinders for the same configuration (zero position) gave a value of $10^{-7}$ which is very close to the exact value. The other quantities of interest for this position of the first tube were checked with the rigid tube results and it was found that they were in very good agreement. This was another validation check of the method employed here.

In the computations of the various Reynolds number flows, the results of one run were used as the initial guess values for the next incremental Reynolds number case (zero-order continuation). This technique allowed a fast convergence of the calculations after four or five Newton–Raphson iterations. A typical computer run for the calculation of the vorticity and the stream function took approximately 90 CPU min on a VAX 11/785 computer. The calculations for

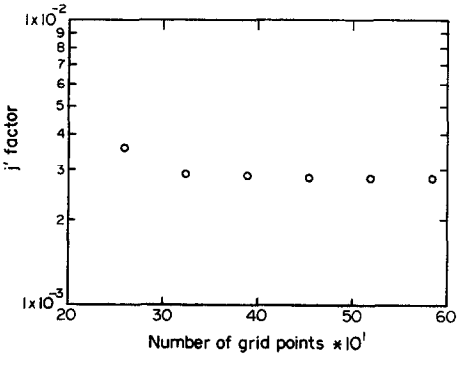


FIG. 3. Grid independence test.

the velocities, temperature and the pressure converged in one iteration and took each approximately 3 CPU min.

Results for the streamlines calculated are shown in Fig. 4 for three Reynolds numbers of 138, 390 and 475 and when the first cylinder is at the 0.2 diameter position. It is seen that asymmetric recirculation zones are developed in the back of the cylinders. These zones become more intense at higher Reynolds numbers.

Figure 5 shows the streamline results for a Reynolds number equal to 218 and for three positions of the first tube at 0.15, 0.25 and 0.35. Again the asymmetric recirculation regions are observed. They become more pronounced with the increase of the first tube eccentricity. Figure 6 shows the constant vorticity lines for the same Reynolds number and for first tube positions of 0.2 and 0.3.

The objective of this study is the calculation of global, time-average quantities of engineering interest for comparison with available experimental data from flexible tube bundles [2]. Hence, the average velocity, pressure and temperature fields were calculated from the results of stream function and vorticity. Figure 7 depicts the variation of the dimensionless pressure along the top symmetry line vs the distance along the computational domain for four transverse positions of the first tube. It is observed that most of the pressure drop occurs at the first cylinder. Also, that the first cylinder pressure drop is more significant when the eccentricity is higher. There is a small amount of pressure recovery behind each tube, a fact which is experimentally observed in tube bundles. Because of partial pressure recovery at the back of the tubes, the decrease of pressure in Fig. 7 is not monotonic.

The time average of the pressure profiles along the top symmetry line vs the longitudinal distance is depicted in Fig. 8 for three Reynolds numbers. The results in this and all the subsequent figures are for

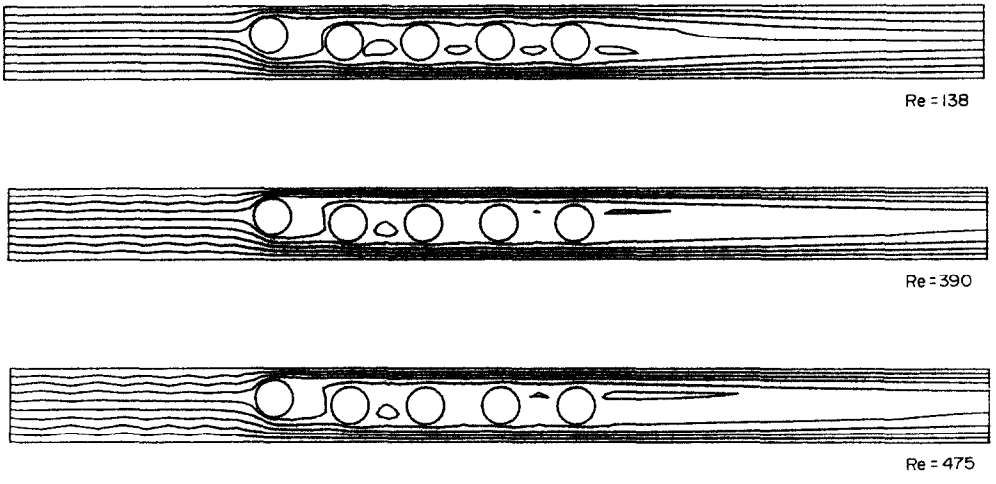


FIG. 4. Streamlines for three Reynolds numbers and the leading cylinder at position 0.2; $\psi_{max} = 1$, $\psi_{min} = 0$, $\delta\psi = 0.1$.

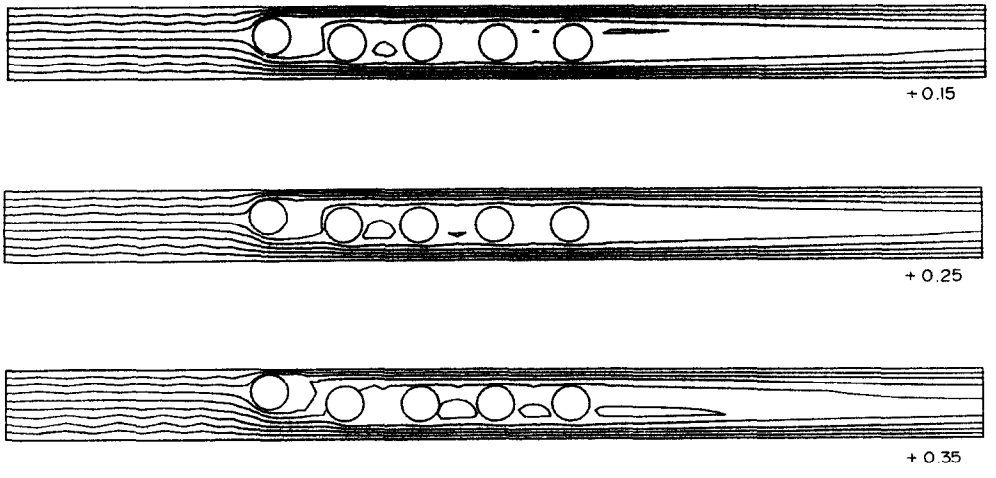


FIG. 5. Streamlines for $Re = 218$ and for three positions of the leading cylinder; $\psi_{max} = 1$, $\psi_{min} = 0$, $\delta\psi = 0.1$.

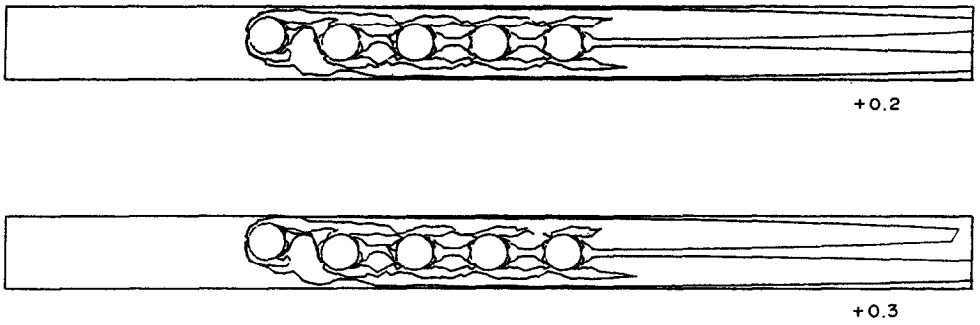


FIG. 6. Constant vorticity lines for two vibrating tube locations; $\omega_{max} = 1$, $\omega_{min} = 0$, $\delta\omega = 0.1$.

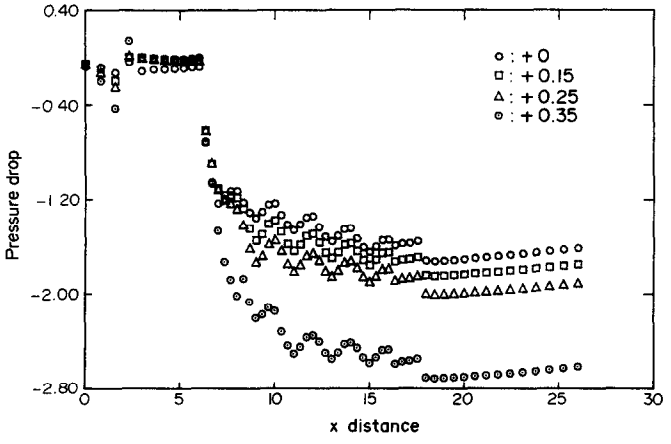


FIG. 7. Pressure profile along the top symmetry line for $Re = 1339$ and for four positions of the leading tube.

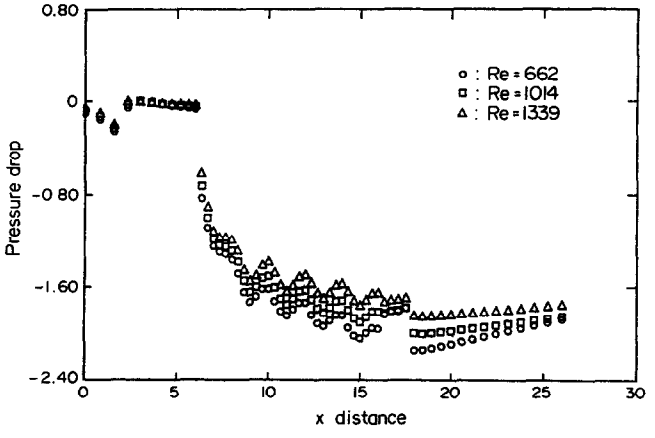


FIG. 8. The influence of Reynolds numbers on the pressure profile along the top symmetry line for the leading cylinder position of 0.2.

pitch to diameter ratios of 2. The average here is taken for all the 15 positions of the first cylinder and according to the quasistatic assumption stated in Section 1 it is the time average pressure profile when the first tube vibrates. Again the profile is not monotonic because of the pressure recovery behind the tubes.

From graphs similar to the above the average pressure drop coefficient $f'$ per row can be obtained. This coefficient is equivalent to an Euler's number for a bundle and is defined as follows:

$$f' = \frac{2\Delta P}{N\rho U^2} \tag{21}$$

where $\Delta P$ denotes the pressure drop over the whole

bundle. The results for $f'$ are plotted in Fig. 9 together with experimental data obtained for two bundles of the same geometry; one of these bundles is made of metal (rigid) tubes and the second is made of Teflon tubes. It is observed that the calculated results show the correct trend of decreasing $f'$ with $Re$. It was also found that the calculated results are within the experimental error of the measured data for the Teflon tubes a fact that supports the validity of the modeling and calculations made in this project.

The effect of the first tube eccentricity on the temperature distribution is shown on Fig. 10 where isotherms are shown for eccentricities of 0.1, 0.25 and 0.35 and a Reynolds number of 218. The major difference here is on the temperature field around the second cylinder. Another point of interest is that the isotherms become more asymmetric as the eccentricity increases.

The local Nusselt number obtained from the temperature field is shown in Fig. 11(a) for a Reynolds number of 540 and an eccentricity of 0.35. It is observed that the first tube has a substantially higher heat transfer coefficient than the rest. However, because of the asymmetric arrangement the second tube shows higher Nusselt numbers than in the rigid tube case [9] and to a lesser extent the third tube. The net effect is a significant increase of the average Nusselt numbers for the whole bundle. The fact that the first row of tubes has higher heat transfer coefficients leads us to believe that heat exchangers should consist of bundles with a few rows placed in series and separated by a distance between them. This was also observed experimentally [2] and can be applied in the design of flexible tube heat exchangers whenever there are no significant space restrictions. The local Nusselt numbers are also plotted for the symmetric (zero eccentricity) case in Fig. 11(b). The results for the symmetric case agreed very well quantitatively and qualitatively [9] with other studies on rigid cylindrical bundles, such as the one in ref. [6].

The global modified Colburn number for the whole bundle vs the Reynolds number is shown in Fig. 12. The experimental data for Teflon tubes are for a five row bundle and the solid tube data pertain to exper-

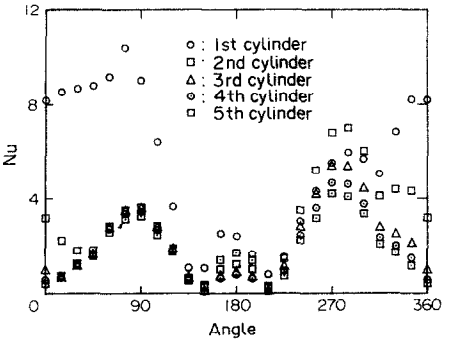


FIG. 11(a). Average local Nusselt number profiles for $Re = 350$ with the leading cylinder vibrating.

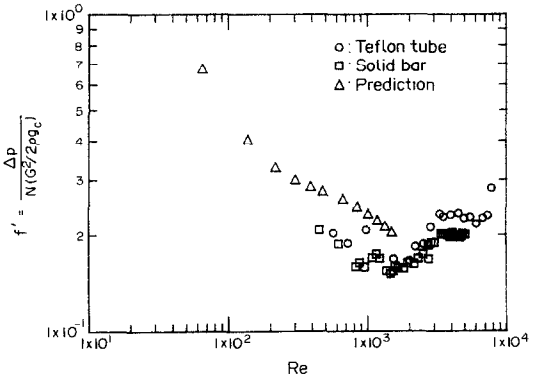


FIG. 9. The average pressure drop coefficient per row and comparison with experimental data.

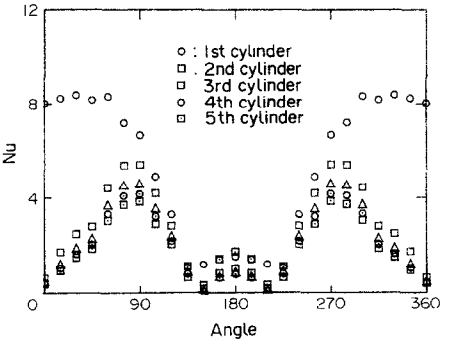


FIG. 11(b). Average local Nusselt number profiles for $Re = 350$ and for rigid cylinders.

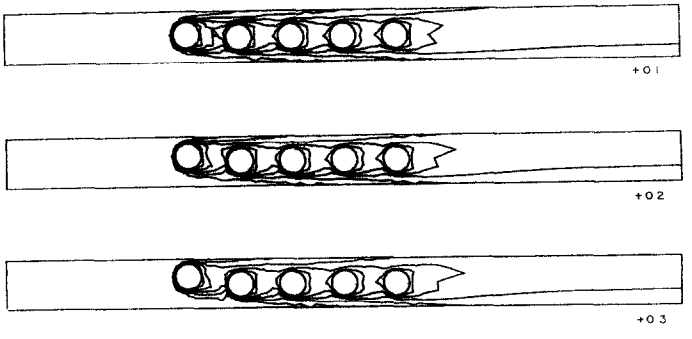


FIG. 10. Isothermal lines for $Re = 218$.

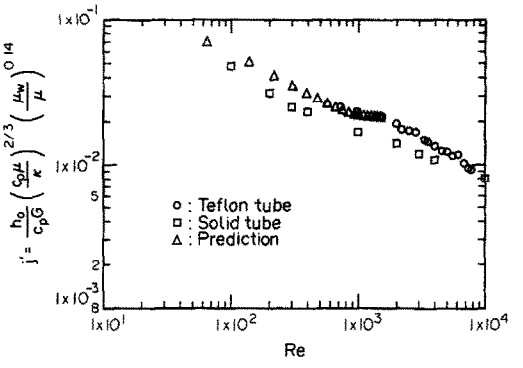


FIG. 12. Average heat transfer coefficients per row in the flexible tube tank.

iments conducted with solid tubes by ESDI (1973). Two observations can be made for this figure. First, the experimental data and the numerical results for the flexible tube bundles agree very well and second that the global heat transfer coefficient for flexible tubes is 20–25% higher than that of the rigid tubes. The first observation is an indication that the present formulation of the problem yields accurate results for the quantities of engineering interest despite the simplifying assumptions in the modeling of this complicated flow and heat transfer problem.

## 5. CONCLUSIONS

Results obtained for the heat transfer and pressure drop coefficients with the method of multiple connected bodies show good agreement with experimental data derived from tube bundles made of flexible Teflon tubes. This indicates that the method used despite its relative simplicity is a good model for the operation of the flexible tube heat exchangers.

It was observed that the eccentricity of the first tube in the row altered significantly the velocity and temperature fields. Local heat transfer and pressure drop coefficients at least for the first two rows depend very much on the eccentricity of the first row of tubes. The local and average transport coefficients increased significantly with the eccentricity of the first tube.

It was observed that the first two tubes caused the major part of the pressure drop and heat transfer in the whole bundle, a fact that was also observed in the rigid tube case. This has the following ramification for the optimal design of flexible tube heat exchangers: it is best to design the heat exchangers with bundles of a few rows, which are placed in series separated by distances allowing sufficient recovery of the flow.

*Acknowledgements*—This study was supported partly by a grant from the DuPont company. Computer time was provided freely by the Department of Mechanical Engineering.

## REFERENCES

1. E. E. Michaelides, Y. Chang and R. T. Bosworth, *Heat and Momentum Transfer Processes through Banks of Flexible Tubes in Air Cross-flow*, A.I.Ch.E. Symp. Series 245, Vol. 81, pp. 109–115 (1985).
2. E. E. Michaelides, Y. Chang and R. T. Bosworth, Heat transfer coefficients and friction factors for banks of flexible vibrating tubes in cross flow, *Proc. 8th Int. Heat Transfer Conf.*, Vol. 6, pp. 2757–2762 (1986).
3. A. C. Mueller, *Experimental Data and Correlations for Tube Banks, in Low Reynolds Number Heat Exchanger Design*. Hemisphere, Washington, DC (1983).
4. S. Kakac, A. E. Bergles and F. Mayinger, *Heat Exchangers*. Hemisphere, Washington, DC (1981).
5. K. A. Antonopoulos, Heat transfer in tube banks under conditions of turbulent inclined flow, *Int. J. Heat Mass Transfer* **28**, 1645–1656 (1985).
6. M. N. Dhaubhadel, J. N. Reddy and D. P. Telionis, Penalty finite element analysis of coupled fluid flow and heat transfer for in-line bundle of cylinders in cross-flow, *Int. J. Non-linear Mech.* **21**, 361–374 (1986).
7. D. P. Telionis and M. S. Romaniuk, Velocity and temperature streaming in oscillating boundary layers, *AIAA J.* **6**, 488–494 (1977).
8. N. Greiner, N. K. Ghaddar, B. B. Mikic and A. T. Patera, Resonant convective heat transfer in grooved channels, *Proc. 8th Int. Heat Transfer Conf.*, Vol. 6, pp. 2867–2872 (1986).
9. Y. Chang, A. N. Beris and E. E. Michaelides, A numerical study of heat and momentum transfer for tube bundles in cross flow, *Int. J. Numer. Meth. Fluids* (1989), in press.
10. Y. Chang, Heat and momentum transfer of flexible tube banks in cross flow, Ph.D. Dissertation, University of Delaware (1988).
11. F. Thomasset, *Implementation of Finite Element Methods for Navier–Stokes Equations*. Springer, New York (1981).
12. G. Strang and G. J. Fix, *An Analysis of the Finite Element Method*. Prentice-Hall, Englewood Cliffs, New Jersey (1973).
13. P. J. Roache, *Computational Fluid Dynamics*. Hermosa, Albuquerque, New Mexico (1972).

## UNE ETUDE NUMERIQUE DU TRANSFERT DE CHALEUR ET DE QUANTITE DE MOUVEMENT POUR UN FAISCEAU DE TUBES FLEXIBLES ATTAQUE TRANSVERSALEMENT

**Résumé**—On développe un schéma numérique pour calculer les coefficients de transfert de chaleur et de perte de charge dans des échangeurs de chaleur avec des tubes flexibles. Les tubes vibrants sont modélisés de façon quasi-statique en donnant au premier tube de la rangée 15 positions asymétriques (avec des excentricités finies), par rapport au repos et en moyennant dans le temps les solutions quasi-statiques qui correspondent à chacune de ces géométries. Les résultats montrent que l'excentricité du premier tube affecte significativement les profils de vitesse et de température. Les coefficients moyens de transfert de chaleur et de perte de pression sont plus élevés que ceux dans le cas des rangées de tubes rigides, symétriquement placés. Une comparaison des résultats présentés montre un très bon accord avec des données expérimentales d'échangeurs thermiques à tubes flexibles.

## NUMERISCHE UNTERSUCHUNG DER WÄRME- UND IMPULSÜBERTRAGUNG AN QUERANGESTRÖMTEN FLEXIBLEN ROHRBÜNDELN

**Zusammenfassung**—Es wird ein numerisches Verfahren zur Berechnung von Wärmeübergang und Druckverlust in Wärmeübertragern aus flexiblen Rohren entwickelt. Die vibrierenden Rohre werden quasistationär modelliert, indem das erste Rohr der Reihe in 15 asymmetrische Positionen (mit definierter Exzentrizität) im Vergleich zu den restlichen Rohren gebracht wird. Die stationären Lösungen für jede dieser Geometrien werden dann zeitlich gemittelt. Die Ergebnisse zeigen, daß die Exzentrizität des ersten Rohres die Geschwindigkeits- und Temperaturprofile erheblich beeinflußt. Die zeitlich gemittelten Wärmeübergangs- und Druckverlustkoeffizienten sind höher als diejenigen im Fall von starren, symmetrisch angeordneten Rohrbündeln. Ein Vergleich der vorliegenden Ergebnisse mit Meßwerten von Wärmeübertragern aus flexiblen Rohren zeigt sehr gute Übereinstimmung.

## ЧИСЛЕННОЕ ИССЛЕДОВАНИЕ ПЕРЕНОСА ТЕПЛА И ИМПУЛЬСА ПРИ ПОПЕРЕЧНОМ ОБТЕКАНИИ ПУЧКОВ ГИБКИХ ТРУБ

**Аннотация**—Разработана численная схема расчета коэффициентов теплопереноса и перепада давления в теплообменниках, выполненных из гибких труб. Вибрирующие трубы моделируются в предположении квазистационарного режима с условием, что первая труба ряда находится в 15 асимметричных (с конечным эксцентриситетом) положениях по отношению к остальным трубам и путем усреднения во времени стационарных решений, соответствующих каждой из этих геометрий. Результаты показывают, что эксцентриситет первой трубы оказывает значительное влияние на профили скорости и температуры. В этом случае усредненные по времени коэффициенты теплопереноса и перепада давления выше значений для жестких симметрично расположенных пучков труб. Полученные результаты хорошо согласуются с экспериментальными данными для теплообменников из гибких труб.